Modelling the EB-PVD thermal barrier coating process: Component clusters and shadow masks

Vitor Emanuel de Matos Loureiro da Silva Pereira, John Rayment Nicholls, Rachel Newton

PII: S0257-8972(16)31342-1
DOI: doi: 10.1016/j.surfcoat.2016.12.054
Reference: SCT 21911

To appear in: *Surface & Coatings Technology*

Received date: 18 October 2016
Revised date: 12 December 2016
Accepted date: 15 December 2016

Please cite this article as: Vitor Emanuel de Matos Loureiro da Silva Pereira, John Rayment Nicholls, Rachel Newton , Modelling the EB-PVD thermal barrier coating process: Component clusters and shadow masks. The address for the corresponding author was captured as affiliation for all authors. Please check if appropriate. Sct(2016), doi: 10.1016/j.surfcoat.2016.12.054

Surface and Coatings Technology, Volume 311, 15 February 2017, pp. 307-313
DOI:10.1016/j.surfcoat.2016.12.054

MODELLING THE EB-PVD THERMAL BARRIER COATING PROCESS: COMPONENT CLUSTERS AND SHADOW MASKS

Vitor Emanuel de Matos Loureiro da Silva Pereira[a]

John Rayment Nicholls[b]

Rachel Newton[c]

[a] Corresponding author: Universidade Lusíada – Norte, *campus* de Vila Nova de Famalicão

Largo Tinoco de Sousa, 4760-108 Vila Nova de Famalicão, Portugal

Phone: +351 252 309 200, Fax: +351 252 376 363

email: v.pereira@fam.ulusiada.pt

[b] Cranfield University

College Road, Cranfield, MK43 0AL, United Kingdom

Phone: +44 (0)1234 754039, Fax: +44 (0)1234 750875

email: j.r.nicholls@cranfield.ac.uk

[c] email: newton.rachel@gmail.com

Abstract

Electron beam-physical vapour deposition (EB-PVD) is a commonly employed process for the production of thermal barrier coatings (TBCs), used in high performance applications such as gas turbines high-pressure aerofoil blades for the aerospace industry. Computer modelling can contribute to improved control of the coating process, important to support a continuous drive for increased efficiency. This paper considers two aspects associated with the EB-PVD coating of TBCs for commercial application: firstly, that clusters of blades are coated simultaneously in commercial coaters and, secondly, that these parts possess a complex geometry, such that shadow masks need to be taken into account. In this context, a computer model that calculates coating thickness distribution along the surface of different engine components, based on the analysis of the vapour deposition flux around complex geometries, is presented. To validate the predictive capability of the computer model two deposition trials were performed. Firstly, a cluster of components was simulated using three rotating cylinders, as a simple representation of coating multiple blades. Secondly, the effect of shadow masks was studied with an arrangement in which flat plates were welded, in the form of a U-shaped component, but with one side shorter than the other. The predicted results generated by the computer model compare favourably with those measured in the experimental runs presented. For the cluster of three cylinders, an error of 4% was obtained whilst the divergence was around 20% for the simulated shadow mask due to the fact that overall coating thickness was significantly reduced. In spite of this, the results obtained from the model were promising with respect to the degree of fit of the inverse square law. It is thought that a virtual source may be responsible for measurements being generally higher than those predicted by the model.

Keywords

Thermal Barrier Coating, Modeling, Simulation, Process Control, Manufacture, EB-PVD

1. Introduction

Engineers have long sought to improve engine efficiency, with thermal barrier coatings developed extensively since the early 1970s by agencies such as NASA and the US Army, within the USA [1–3], and through similar initiatives within Europe, funded by the Commission of the European Communities (BriteEuram and COST) [4] as well as being applied commercially for decades [5]. The prime function of thermal barrier coatings is to insulate components, such as superalloy turbine blades and vanes operating at elevated temperatures, from the harsh combustion gases present in such environments. The potential temperature reduction that can be obtained is greater than the cumulative gains that have been made in the temperature capability of superalloys, which thus allows a significant increase in thermal efficiency and/or increase in component durability [5].

Engine efficiency is directly linked to the temperature at which the gases are burnt in the combustion process. Hence there is a strong incentive to raise this temperature. Indeed, Clarke et al. [6] have charted the significant progress in engine efficiency that TBCs have allowed since the late 1960s. They also emphasized the important role that modelling can play in supporting future improvements, since the drive for increasing efficiency continues. The integral role of modelling has also been highlighted by other authors [7–12].

The coating process employed is important because it affects economics and coating microstructure, hence influencing coating properties such as thermal conductivity, coefficient of thermal expansion (CTE), bonding, coating durability, and other important coating properties [13,14]. Thermal barrier coatings on aeroturbine blades are commonly applied by the electron beam-physical vapour deposition (EB-PVD) process [15]. In this process, an electron beam is focused onto the surface of the material to be evaporated (usually a solid ingot), the material melts and then evaporates, with atoms depositing onto the substrate

surface and building up the coating [16]. These coatings contain expensive rare earth materials such as yttria-stabilised zirconia and components have a complex shape, with most turbine aerofoils having many small holes with a diameter between 250 μm and 1 mm. Therefore, predicting the thickness distribution across the whole surface is vital to reduce the large sums of money which could be wasted in scrap components. Further, since EB-PVD is a line of sight process, shadowing can occur leading to changes in microstructure such as that often referred to as "feather arms" in which the porosity is more open and thermal conductivity decreases [17]. It is also desirable to vary the thermal barrier coating thickness around the component for best aerodynamic performance, with a thicker TBC on the leading edge, thinning towards the trailing edge of the aerofoil. Hence, "shadow masks" are employed to overcome this issue [13]. Also, in addition to rotating and tilting actions, commercial EB-PVD chambers coat multiple blades in each batch [18].

Models can support the prediction of coating thickness, morphology, column inclination and surface roughness both around a component and from component to component, which can facilitate the reproducible manufacture of TBC coated components. Various models capable of predicting vapour deposition have been discussed in the literature [7,19–22]. Modelling of the degradation or failure mechanisms has also received attention [12,23–26].

2. Model overview and experimental

Well-known scientists such as Heinrich Hertz, Martin Knudsen and Irving Langmuir were some of the first researchers to investigate the transition of solids or liquids into the gaseous state using the laws of thermodynamics. It is now well established that the directionality of evaporation molecules in vacuum at low rates from a small area source leads to a thickness distribution on a flat surface that follows a law stating that the mass per unit area deposited on a surface element is equal to [27,28]:

$$\frac{dM}{dA} = \frac{M_e}{\pi h^2}\cos^{\mathrm{n}}\theta\cos\alpha$$

where M_e is the total mass evaporated, θ is the angular displacement of the substrate relative to the normal to the source, n is a coefficient that defines the focus of the source, α is the inclination of the substrate to the line of vapour flux, measured from the normal of the substrate, and h is the source-to-substrate distance, as illustrated in Fig. 1.

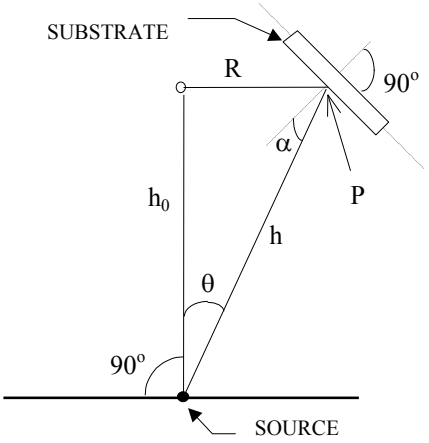

Fig. 1. Schematic representation of geometry of evaporation.

However, this simple rule is characteristic only when the source behaves as a single-point evaporator or, in other words, when the vapour-emitting surface is a small area compared to the source-to-substrate distance. For the more general case, the thickness deposited is related to the rate of deposition from all sources and the deposition time such that the thickness distribution of a thermally evaporated coating, deposited from an ideal point source evaporator, follows an inverse square law governed by an equation of the form [27,29,30]:

$$\frac{d}{d_0} = \frac{h_0^2}{h^2}\cos^{\mathrm{n}}\theta\cos\alpha$$

where d is the coating thickness at a distance h from the vapour source, d_o is the thickness directly over the vapour flux at a distance h_o from the source, and α, θ and n defines the

source to substrate geometry and the evaporation characteristics of the source, as mentioned previously.

Gas turbine aerofoils have an elaborate geometry and are designed using advanced CAD software. The geometric information about the substrate is thus available for inclusion in the computer model and can be exported to a file from the CAD software. The simple and commonly available STL (STereoLithography) file format, widely used for rapid prototyping, 3D printing, and computer-aided manufacturing, was chosen for interchanging data between CAD systems and the computer model. STL files describe only the surface geometry of a 3D component using a mesh of triangles (called facets). Each facet is described by a unit normal (a perpendicular vector with a length of 1.0) and three points representing the vertices (corners) of the triangle.

In addition to an accurate representation of the substrate and shadow-mask (if used), both the system configuration (source to substrate distance, and vapour incidence angle, for example) and the rotating fixture configuration (e.g. rotational speed, centre of rotation, and axis of rotation) are needed.

This paper uses a true line-of-sight computer model, based on the previously mentioned inverse square law, to predict thickness distribution deposited from a single point source evaporator [16,31]. In these works, various evaporation characteristics, such as source-to-substrate distance, vapour incidence angle, substrate rotation, and evaporation rate, have been accommodated by developing a generalised point source evaporation model.

The main procedure of the computer model calculates the total coating thickness at each facet of the triangulated substrate model. Firstly, a substrate model in STL format must be selected and, then, the system configuration should be specified (for a rotating component, for instance, both the point of rotation and vector of rotation are necessary). Following this, the

model uses a loop repeated once for each facet of the STL file. Each iteration of the loop involves calculating the new facet position, determining whether the facet is visible and, if so, calculating the incremental increase in coating thickness based on the system parameters (i.e. inclination of the substrate and source-to-substrate distance). This visibility issue is critical in the optimisation of shadow mask positions.

To validate the predictive capability of the computer model two deposition trials using an EB-PVD laboratory coater were performed. The coater equipment consists of a vacuum chamber, an electron-beam gun (EB-gun), a substrate jigging for holding the components to coat, and a source with the evaporator material, as illustrated in Fig. 2.

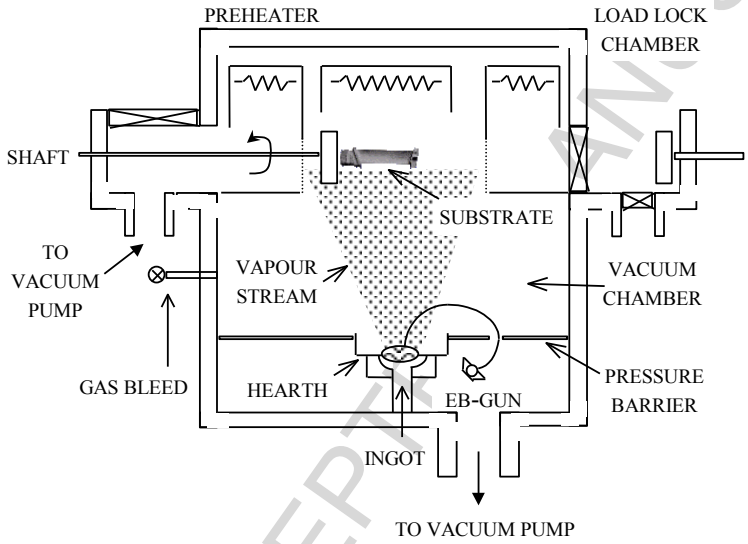

Fig. 2. Schematic diagram of a commercial EB-PVD coater system [31].

Table I presents a detailed description of the specifications of the EB-PVD laboratory coater used for the physical experiments. The stated upper chamber gas pressure is the gas pressure only (argon + oxygen) and was measured with a Baratron gauge within the vacuum chamber but remote from the furnace cavity. The vapour flux was more localised within the furnace cavity, which was thermally insulated from the externally cooled chamber walls. The pressure was measured remotely from the furnace cavity, but within the vacuum chamber. The open

design (no baffles restricting pumping) would mean the pressure of the gas at 1000°C and in the vacuum chamber, but away from the furnace cavity, would be the same.

The vapour source melts locally, directly where the beam impinges, over an area 2 cm in diameter. The scan pattern is set such that the rotating source rod passes through this area ensuring the whole of the top of the rod is molten at some time in the rod's rotation. The dimensions of this melt pattern remained essentially constant during each deposition run, so there are both no obvious changes in the shape of the vapour plume or local emissions. The typical evaporation rate was between 4-6 μm/min; thus a deposition would take 20 minutes once the substrate was stabilised at temperature. All reasonable steps have been taken to ensure that all processing parameters were kept as stable as realistically possible. For example, the rod was raised from time to time in order to maintain a constant source-to-substrate distance.

Run I addressed a cluster of components while Run II studied the effect of shadow masks.

After deposition, samples were prepared by metallographic sectioning and then coating thicknesses were measured directly by computerised planimetry using the Leica Q500MC system, an easy-to-use optical microscopy and image processing and analysis system. The image analysis software package Quantitative Interactive Programming language (QUIPS), running under the Microsoft Windows environment, was used to control the hardware system. Using the component from Run I as an example – cylinders with 0.8 cm in diameter –, the software calculates, from a given set of positions, the centre point of the cylinder and its radius. Then, based on the centre point, the system moves a motorised stage automatically, allowing the user to take equally spaced radial coating thicknesses measurements around the component. The repeatability of these measurements was typically ±3 μm in any location

from measurements of adjacent positions. From sample to sample – repeat runs – the repeatability was typically ±7 μm for the same location.

Table I: Specifications of the laboratory EB-PVD coater

Volume	≈ 0.3 m^3
Number of Sources	1
Source Diameter	38 mm
Source Height	20 cm
Pressure (upper chamber)	1×10^{-2} mbar
Pressure (lower chamber)	5×10^{-4} mbar
Gun Acceleration Voltage	10 kV
Current	0.6 A
Power	6 kW
Substrate Temperature	1000ºC
Gas Flow	Ar-10%O_2 (50 cc/min^{-1})

2.1 Run I: Cluster of components

To be economic, the coating industry must coat multiple blades per coating session. This is important because it not only increases the throughput of the coating equipment, but also reduces unit coating cost. The ideal arrangement of the cluster is such that the blades limit the deposition on the trailing edge of other blades (act as a shadow-mask) whilst not masking the leading edge of the component. One solution could be the position of, for instance, identical blades at 120º angular displacement (for a cluster of three blades) with their trailing edges pointing to the centre of the circle and their leading edges pointing away from the centre of the imaginary circle (Fig. 3). The computer model allows for this arrangement to be

investigated by predicting the modification in coating thickness as a function of the distance of blades from the centre of rotation and rotational speed.

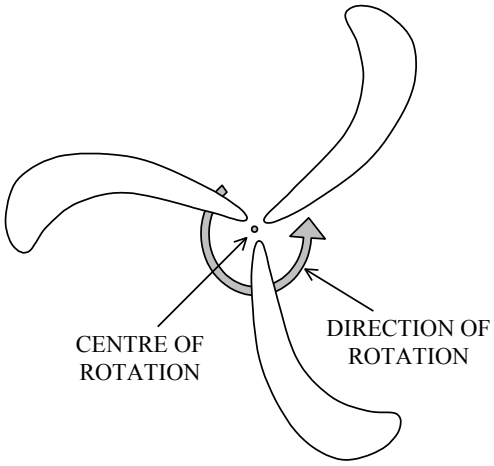

Fig. 3. Schematic representation of a cluster of three blades.

To explore this geometry, a model substrate system, based on three rotating cylinders was studied, as a simple representation of blades. This configuration allowed the feasibility of coating a cluster of blades to be evaluated. Three pins were welded to a 6 cm diameter disc in order to study both the rotational and shadowing effects on the thickness distribution. The pins were 0.8 cm in diameter and 10 cm long positioned in a circle 1.5 cm away from the centre of the disc and at an angular separation of 120º. Fig. 4 shows the wireframe view of the STL file for the cluster of three pins arrangement. Two triangulated views of the arrangement, one as generated by the CAD/STL translator using a tolerance of 0.8 mm, and the other one with a sixfold increase in the number of triangles (a process called tessellation), performed by the software tool, are shown in Fig. 5.

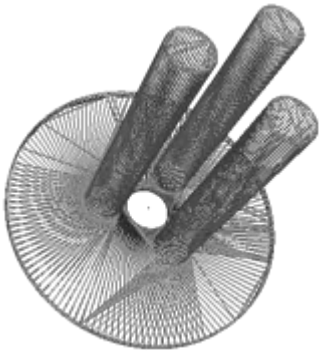

Fig. 4. Wireframe view of a three-pin cluster arrangement.

a) 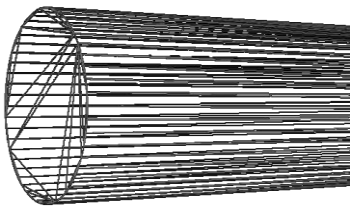

b) 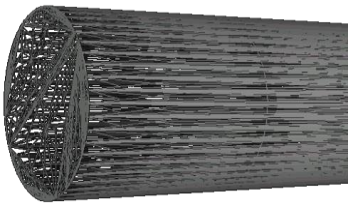

Fig. 5. Detailed view of the end of a pin showing the difference in spatial resolution between the (a) default tolerance component and (b) a model with a 6× increase in the number of triangles, performed by the computer model.

The centre of the disc was used as the point of rotation of the structure. In addition, the vector of rotation was parallel to the disc's normal, i.e. parallel to the pins. A rotational speed of 20 rpm was used. As previously mentioned, this arrangement is of interest because turbine blades can be positioned with their trailing edge pointing to the centre of the disk, in order to limit the coating thickness, whereas the leading edge, which points away from the other two blades, does not get shadowed by the adjacent blades.

2.2 Run II: The effect of shadow mask design

For good aerodynamic performance, aerofoil coating thickness is not uniform, but rather the coating on the trailing edge of aerofoil components is limited to a few tens of microns, while the coating on the leading edge may be around 125-250 μm thick, depending on application. It follows, therefore, that the modelling of the deposition should allow shadow masks to be positioned relative to the substrate and the coating thickness calculated for the combined arrangement, based on the influence of the shadow-mask. As with any substrate, these fixtures could be produced by CAD software and exported to an STL file for use in the computer

program. It is thus apparent that good masking design can have a significant effect on the cost and efficiency of a coating operation.

Run II investigated the effect of shadow masks on the thickness profile with an arrangement in which flat plates were welded, roughly resembling a U-shaped component, but with one side smaller than the other. One plate behaves as the component while the other is the shadow-mask. Fig. 6 shows the wireframe view of the STL file of this component.

It is worth noting that because all surfaces were flat, the CAD/STL generator only required two triangles to approximate each surface, regardless of the tolerance specified. For this reason, the computer program was used once again to increase the mesh of the triangles in order to provide a better accuracy in the predicted values. In addition to the study of the masking effect, this structure also allowed the degree of fit of the inverse square law to be investigated by analysing areas not shadowed by the mask.

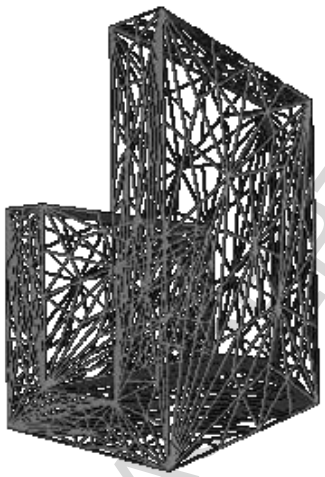

Fig. 6. Shadow-mask arrangement with a 36× increase in the number of triangles.

The coating thickness was measured around a section profile, and the predicted values calculated using the computer model. The predicted coating thickness was calculated by positioning the substrate within the computer model's coating space in order to match the expected component movement. Rotation of the substrate involved 72 iterations (5º

increments) around the longitudinal centre of the larger plate. Fig. 7 presents this configuration with sides named from Side A to Side E in order to facilitate the presentation of results.

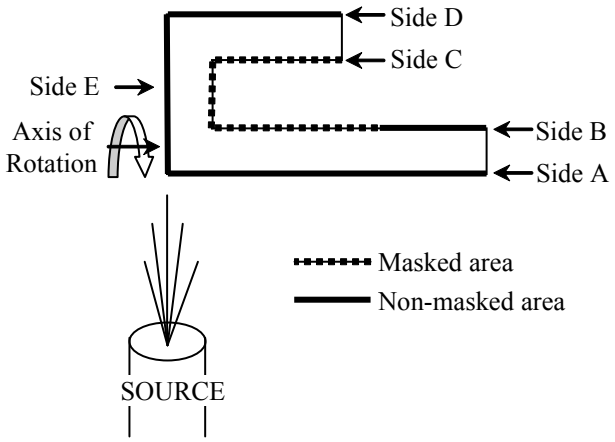

Fig. 7. Configuration of the masking effect substrate.

3. Results and discussion

3.1 Run I: Cluster of components

For this experimental run the point of rotation was 15 cm above the source. Since the cylinders were 8 mm in diameter and 1.5 cm away from the centre of the disk, the closest and the furthest away the surfaces of the cylinders get to the source were 13.1 cm and 16.9 cm, respectively. This is important because, for instance, for a normalised deposition rate of 100% at 15 cm above the source, the computer model predicts a deposition rate of 131.1% and 78.8%, respectively for these two heights (using the inverse square law, these rates are calculated as $\frac{1}{\left(\frac{\text{height}}{15}\right)^2}$, assuming a position directly above de source, $\theta = 0$, and a vapour flux normal to the substrate, $\alpha = 0$). In other words, the coating thickness for a rotating cluster of blades changes not only because the inclination of the substrate changes, but also because the source-to-substrate distance also changes considerably.

Due to the simultaneous rotation and shadowing effect, the deposition rate predicted and measured for the shadowed areas closest to the centre of the disk was relatively low compared to areas not affected by shadowing. Fig. 8 shows a macro photograph of the cluster of three pins after deposition.

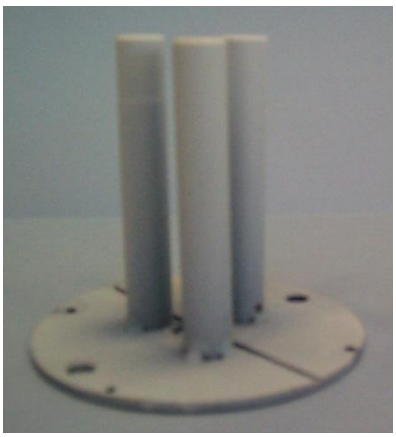

Fig. 8. Macro photograph of the cluster of three pins after deposition.

Two samples from the experimental run were analysed and the coating thickness measured all around the circular profile, with angular displacement varying from 0º to 360º, with 0º being the point on the cross-section of the cylinders facing away from the centre of the cluster and 180º the point closest to the centre of the cluster. Both samples were taken from the same pin (they were positioned 1 and 3 cm from the end of the pin, respectively). Fig. 9 presents a comparison between measured and predicted deposition profiles. In addition, it illustrates the thickness distribution around the specimens as a function of angular displacement from the 0º reference point. Values 0º and 180º represent the points of highest and lowest deposition, respectively. Fig. 9 further shows that the predicted coating thickness for the point of lowest deposition (point affected by the shadowing) is approximately 50% that of the point of highest deposition.

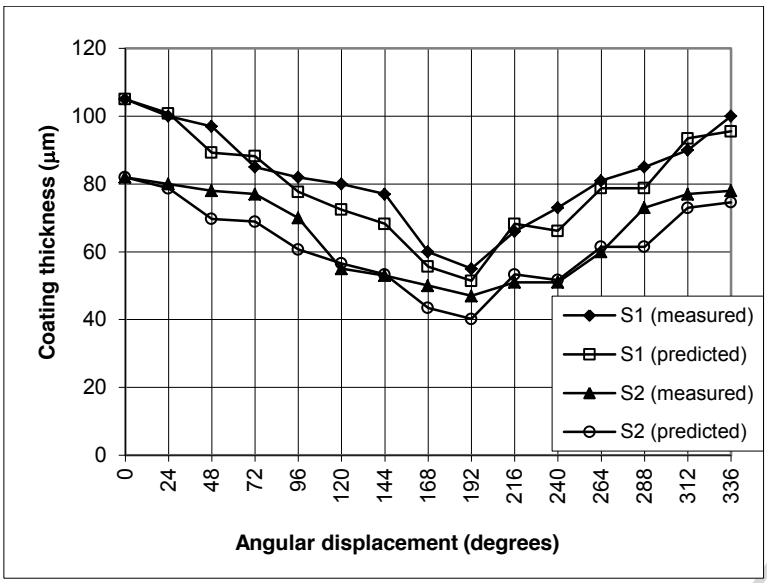

Fig. 9. Comparison between measured and predicted deposition profiles for two samples (S1 and S2) in a cluster of cylinders.

Fig. 10 demonstrates the degree of fit between measured and predicted results, irrespective of angular displacement and source-to-substrate distance. A perfect fit would be the diagonal straight line included in the figure. Agreement of the predicted coating thickness with the measured thickness is good. The coating thickness can be modelled to within an accuracy of around 4%, i.e. a standard deviation of ±2%, for this example. Fig. 10 further illustrates that the measured thickness is generally higher than that predicted, which may reflect the existence of virtual source within the coater that is not taken into account with this multiple point source evaporation model. A virtual source is a more densely distributed region of evaporated material directly over the ingot, in which viscous flow can occur due to the equilibrium vapour pressure of the charge [32]. Such a region of viscous flow acts like an isotropic emitter, with the point from which material appears to emit called the virtual source. Fig. 9 would imply this virtual source would only introduce a small effect. Equally, from Fig. 11 one may infer that any effect of such a virtual source would be less than 10% of the predicted vapour flux.

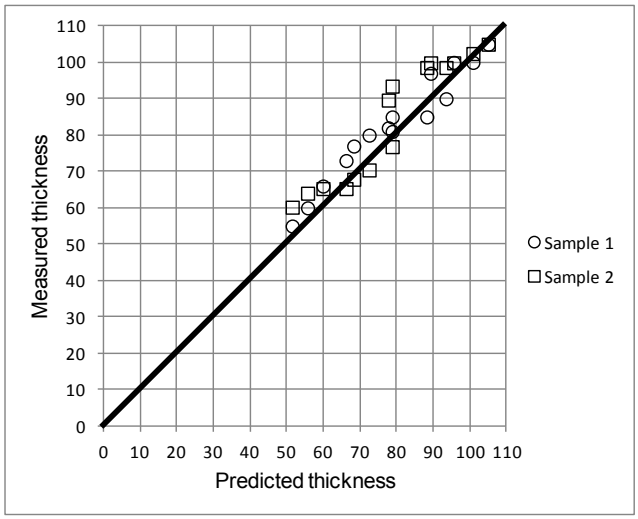

Fig. 10. Scatter diagram presenting a comparison between predicted and measured results.

3.2 Run II: The effect of shadow mask design

The effect of shadow masks on the thickness profile was addressed by using the arrangement illustrated in Fig. 7, in which masked and non-masked areas are perpendicular to the source. In addition to the study of the masking effect, this structure also allowed the degree of fit of the inverse square law to be investigated by analysing areas not shadowed by the mask.

The coating thickness was measured around a section profile, and the predicted values calculated using the computer model. The predicted coating thickness was calculated by positioning the substrate within the computer model's coating space in order to match the expected component movement.

From Fig. 7 it is clear that SIDE A and SIDE D were not subjected to any shadowing effect, in addition to part of SIDE B, represented as a solid thick line. On the other hand, for SIDE C and part of SIDE B the expected thickness profile was modified by the shadow mask. Fig. 11 shows a comparison of thickness (measured and predicted) versus linear displacement for the various sides. SIDE D and SIDE E have the highest coating due to the fact that they are not masked and get closer to the source than all other sides. Because SIDE A, SIDE D, and SIDE

E are not affected by the shadow-mask, the coating thickness increases as the source-to-substrate distance decreases; for SIDE B, however, the opposite occurs because of the shadowing effect. As expected, part of SIDE B and SIDE C, affected by the shadow-mask, exhibit a measured coating thickness higher than that predicted, which may reflect the existence of virtual source, as with Run I. Worth noting is that a thin coating, around 10-15 μm thick, was measured on the masked area of SIDE B and all SIDE C.

Fig. 11. Comparison between measured and predicted deposition profiles around the shadow-mask arrangement.

Fig. 12 presents a comparison between predicted and measured results irrespective of source-to-substrate distance. While the difference between the model and the measured values is greater than for Run I (around 20%), this is most likely to be, at least in part, due to the fact that the overall coating thickness is much lower. This emphasises the fact that further experimental research is required in order to quantify the effect of shadow-masking. As can be seen from Fig. 11, the lowest coating was measured for the areas affected by the shadow-mask; from Fig. 12 it is evident that the measured coating thickness for these areas was higher than that predicted, which is consistent with Run I.

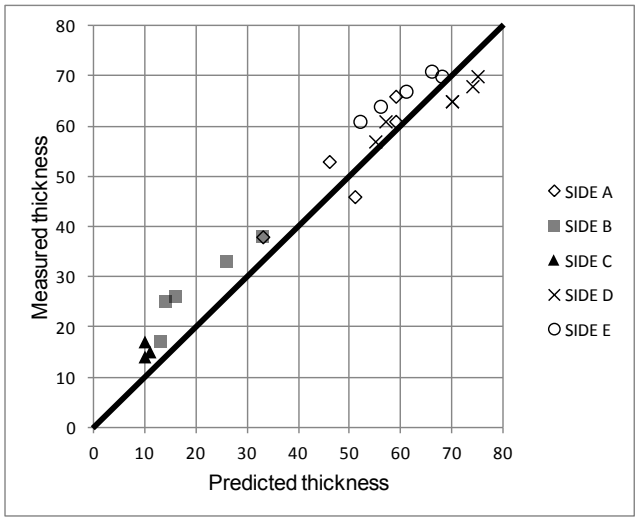

Fig. 12. Scatter diagram demonstrating the degree of fit for the shadow mask arrangement.

4. Conclusion

Further tests were presented to validate a previously developed computer model that predicts coating thickness distribution along a component deposited from a single point source evaporator. The computer model predicts thickness profile on components, provided their geometric information is specified by an STL file, which can be generated from CAD software.

Two experiments have verified the validity of the model in predicting coating thickness with respect to two important aspects for coating aerofoil blades. The first experiment used a cluster of three rotating cylinders, as a simple representation of coating multiple blades. The second assessed the effect of shadow masks on the thickness profile with an arrangement in which flat plates were welded, forming approximately a U-shaped component, but with one side smaller than the other.

For the cluster of three cylinders, the model showed an overall good agreement with the measured thickness, with an error of 4% (±2 standard deviations). It is thought that the

presence of a virtual source, directly above the source, may be responsible for measurements being generally higher than those predicted by the model.

Results obtained for the experiment investigating the effect of shadow masks on the thickness profile are subject to greater divergence from those predicted by the model (around 20%). This may be explained by the fact that the overall coating thickness was much lower. In spite of this, the results obtained from the model were promising with respect to the degree of fit of the inverse square law.

Acknowledgment

We would like to thank EPSRC for the financial support provided for the development of the model on which this work was based.

5. References

[1] S.J. Dapkunas, R.L. Clarke, Evaluation of the hot-corrosion behavior of thermal barrier coatings, (1974). https://trid.trb.org/view.aspx?id=31260 (accessed July 21, 2016).

[2] C.H. Liebert, R.E. Jacobs, S. Stecura, C.R. Morse, Durability of zirconia thermal-barrier ceramic coatings on air-cooled turbine blades in cyclic jet engine operation, (1976). http://ntrs.nasa.gov/search.jsp?R=19760025104 (accessed July 21, 2016).

[3] S. Stecura, Two-layer thermal barrier coating for turbine airfoils-furnace and burner rig test results, (1976). http://ntrs.nasa.gov/search.jsp?R=19760024242 (accessed July 21, 2016).

[4] D. Coutsouradis, Centre de recherches métallurgiques, Commission of the European Communities, eds., High temperature alloys for gas turbines, Applied Science Publishers, London, 1978.

[5] S.M. Meier, D.K. Gupta, K.D. Sheffler, Ceramic thermal barrier coatings for commercial gas turbine engines, JOM. 43 (1991) 50–53. doi:10.1007/BF03220164.

[6] D.R. Clarke, M. Oechsner, N.P. Padture, Thermal-barrier coatings for more efficient gas-turbine engines, MRS Bull. 37 (2012) 891–898. doi:10.1557/mrs.2012.232.

[7] K.S. Fancey, A coating thickness uniformity model for physical vapour deposition systems: further analysis and development, Surf. Coat. Technol. 105 (1998) 76–83.

[8] I. Fuke, V. Prabhu, S. Baek, Computational Model for Predicting Coating Thickness in Electron Beam Physical Vapor Deposition, J. Manuf. Process. 7 (2005) 140–152. doi:10.1016/S1526-6125(05)70091-8.

[9] A.S. James, A. Matthews, A simple model for the prediction of coating thickness uniformity from limited measured data, Surf. Coat. Technol. 61 (1993) 282–286. doi:10.1016/0257-8972(93)90239-K.

[10] V. Kumar, K. Balasubramanian, Progress update on failure mechanisms of advanced thermal barrier coatings: A review, Prog. Org. Coat. 90 (2016) 54–82. doi:10.1016/j.porgcoat.2015.09.019.

[11] V. Kumar, B. Kandasubramanian, Processing and design methodologies for advanced and novel thermal barrier coatings for engineering applications, Particuology. 27 (2016) 1–28. doi:10.1016/j.partic.2016.01.007.

[12] L. Wang, D.C. Li, J.S. Yang, F. Shao, X.H. Zhong, H.Y. Zhao, K. Yang, S.Y. Tao, Y. Wang, Modeling of thermal properties and failure of thermal barrier coatings with the

use of finite element methods: A review, J. Eur. Ceram. Soc. 36 (2016) 1313–1331. doi:10.1016/j.jeurceramsoc.2015.12.038.

[13] P.L. Fauchais, J.V.R. Heberlein, M. Boulos, Thermal Spray Fundamentals: From Powder to Part, Springer Science & Business Media, 2014.

[14] C.U. Hardwicke, Y.-C. Lau, Advances in Thermal Spray Coatings for Gas Turbines and Energy Generation: A Review, J. Therm. Spray Technol. 22 (2013) 564–576. doi:10.1007/s11666-013-9904-0.

[15] R. Darolia, Thermal barrier coatings technology: critical review, progress update, remaining challenges and prospects, Int. Mater. Rev. 58 (2013) 315–348. doi:10.1179/1743280413Y.0000000019.

[16] J.R. Nicholls, V. Pereira, K.J. Lawson, D.S. Rickerby, Process control of deposition profiles in the manufacture of EB-PVD thermal barrier coatings, in: NATOs Res. Technol. Organ. Meet. Proc. 9, Brussels, Belgium, 1998: p. 16.1-16.11.

[17] ACerS, Progress in Thermal Barrier Coatings, John Wiley & Sons, 2009. https://books.google.pt/books/about/Progress_in_Thermal_Barrier_Coatings.html?hl=pt-PT&id=WpcmRsBsKKgC.

[18] A. Feuerstein, J. Knapp, T. Taylor, A. Ashary, A. Bolcavage, N. Hitchman, Technical and Economical Aspects of Current Thermal Barrier Coating Systems for Gas Turbine Engines by Thermal Spray and EBPVD: A Review, J. Therm. Spray Technol. 17 (2008) 199–213. doi:10.1007/s11666-007-9148-y.

[19] K. Bobzin, E. Lugscheider, R. Nickel, Modeling and simulation in the production process control and material property calculation of complex structured EB-PVD TBCs, Comput. Mater. Sci. 39 (2007) 600–610. doi:10.1016/j.commatsci.2006.08.011.

[20] S. Bosch, Lens coating in thermal evaporation physical vapour deposition chambers: optimization of the geometrical configuration, J. Phys. Appl. Phys. 26 (1993) 124. doi:10.1088/0022-3727/26/1/020.

[21] T.M. Rodgers, H. Zhao, H.N. Wadley, Vapor deposition on doublet airfoil substrates: Coating thickness control, J. Vac. Sci. Technol. A. 33 (2015) 061509.

[22] U. Schulz, S.G. Terry, C.G. Levi, Microstructure and texture of EB-PVD TBCs grown under different rotation modes, Mater. Sci. Eng. A. 360 (2003) 319–329. doi:10.1016/S0921-5093(03)00470-2.

[23] S. Baek, V. Prabhu, Simulation model for an EB-PVD coating structure using the level set method, J. Manuf. Process. 11 (2009) 1–7. doi:10.1016/j.jmapro.2009.05.001.

[24] L. Deng, Y. Xiong, P. Xiao, Modelling and experimental study of impedance spectra of electron beam physical vapour deposition thermal barrier coatings, Surf. Coat. Technol. 201 (2007) 7755–7763. doi:10.1016/j.surfcoat.2007.03.012.

[25] A. Gupta, M. Talha, Recent development in modeling and analysis of functionally graded materials and structures, Prog. Aerosp. Sci. 79 (2015) 1–14. doi:10.1016/j.paerosci.2015.07.001.

[26] R.G. Wellman, J.R. Nicholls, A Monte Carlo model for predicting the erosion rate of EB PVD TBCs, Wear. 256 (2004) 889–899. doi:10.1016/j.wear.2003.09.001.

[27] R.F. Bunshah, Deposition technologies for films and coatings: developments and applications, Noyes Publications, 1982.

[28] E. Lang, Coatings for High Temperature Applications, Applied Science Publishers, 1983.

[29] L.I. Maissel, R. Glang, Handbook of thin film technology, McGraw-Hill, 1970.

[30] J.L. Vossen, W. Kern, Thin Film Processes, Academic Press, 1978.

[31] V. Pereira, R. Silva, J. Nicholls, Computer model to predict evaporation and deposition of thermal barrier coatings, Aerosp. Sci. Technol. 10 (2006) 442–448. doi:10.1016/j.ast.2006.01.005.

[32] R.J. Hill, Physical Vapor Deposition, Temescal, 1986.

Highlights

A computer model to predict EB-PVD TBC coating thickness profile is validated.

The model incorporates the component's geometric information as an STL file.

A three-pin cluster was used to model a blade cluster, with an error of around 4%.

A U-shaped component tested the use of shadow masks to an accuracy of 20%.

A virtual source may be responsible for higher than predicted measurements.

Modelling the EB-PVD thermal barrier coating process: Component clusters and shadow masks

de Matos Loureiro da Silva Pereira, Vitor Emanuel

2016-12-18

Vitor Emanuel de Matos Loureiro da Silva Pereira, John Rayment Nicholls and Rachel Newton. Modelling the EB-PVD thermal barrier coating process: Component clusters and shadow masks. Surface and Coatings Technology, Volume 311, 15 February 2017, pp. 307-313
http://dx.doi.org/10.1016/j.surfcoat.2016.12.054